HHS Public Access

Author manuscript

J Neurosci Methods. Author manuscript; available in PMC 2018 June 01.

Published in final edited form as:

J Neurosci Methods. 2017 June 01; 284: 103–111. doi:10.1016/j.jneumeth.2017.04.009.

An Information Theory Framework for Dynamic Functional Domain Connectivity

Victor M. Vergara, PhD[1], **Robyn Miller, PhD**[1], and **Vince Calhoun, PhD**[1,2]

[1]The Mind Research Network and Lovelace Biomedical and Environmental Research Institute, 1101 Yale Blvd. NE, Albuquerque, New Mexico, 87106

[2]Department of Electrical and Computer Engineering, University of New Mexico, Albuquerque, New Mexico, 87133

Abstract

Background—Dynamic functional network connectivity (dFNC) analyzes time evolution of coherent activity in the brain. In this technique dynamic changes are considered for the whole brain. This paper proposes an information theory framework to measure information flowing among subsets of functional networks call functional domains.

New Method—Our method aims at estimating bits of information contained and shared among domains. The succession of dynamic functional states is estimated at the domain level. Information quantity is based on the probabilities of observing each dynamic state. Mutual information measurement is then obtained from probabilities across domains. Thus, we named this value the cross domain mutual information (CDMI).

Results—Strong CDMIs were observed in relation to the subcortical domain. Domains related to sensorial input, motor control and cerebellum form another CDMI cluster. Information flow among other domains was seldom found.

Comparison with existing methods—Other methods of dynamic connectivity focus on whole brain dFNC matrices. In the current framework, information theory is applied to states estimated from pairs of multi-network functional domains. In this context, we apply information theory to measure information flow across functional domains.

Conclusion—Identified CDMI clusters point to known information pathways in the basal ganglia and also among areas of sensorial input, patterns found in static functional connectivity. In contrast, CDMI across brain areas of higher level cognitive processing follow a different pattern that indicates scarce information sharing. These findings show that employing information theory to formally measured information flow through brain domains reveals additional features of functional connectivity.

Corresponding Author: Victor M. Vergara, The Mind Research Network and Lovelace Biomedical and Environmental Research Institute, 1101 Yale Blvd. NE, Albuquerque, New Mexico, 87106, Telephone: 505-272-5028, Fax: 505-272-8002, vvergara@mrn.org.

Keywords

functional MRI; resting state network; functional connectivity; alcoholism; nicotine addiction; dynamic functional network connectivity; entropy; mutual information

Introduction

Brain functional connectivity has revealed important relationships among spatially distributed brain networks. Distinctive patterns of resting state functional connectivity have been observed among patients with bipolar and major depressive disorder (He et al., 2016), addictive substance users (Sutherland et al., 2012), schizophrenia and other brain illnesses (Fox et al., 2010). Existing analyses tend to view the brain in either fine spatial segregation with coarse time averaging or coarse spatial and finer time scales. More recently there has been interest in analyzing sets of brain networks grouped by broad functional categories called domains (Miller et al., 2016a). The study of functional domains increases interpretability and allows the extraction of additional information.

Functional connectivity studies, which are derived from functional magnetic resonance imaging (fMRI) data, have revealed the existence of resting state networks (RSN) that are characterized by their temporally coherent activation patterns (van den Heuvel et al., 2009). Many of these observations have been obtained using correlation measures over relatively long periods of time (five minutes or longer) and overlooking behavior at finer time scales (Allen et al., 2011; Erhardt et al., 2011). Dynamic functional network connectivity (dFNC) is a technique that overcomes time scale limitations by analyzing short time synchronous behavior (Allen et al., 2012; Sakoğlu et al., 2010). The whole brain synchronous state is estimated at each time step using all RSNs. However, temporal changes at more functionally localized scales can be lost in this type of analysis.

The current work introduces a method to analyze dynamic functional connectivity changes among biologically defined RSN domains. RSNs within a domain tend to relate to each other based on functional considerations (Buckner et al., 2008; van den Heuvel et al., 2009). We will name our method dynamic functional domain connectivity (dFDC) because it focuses on evaluating domain information. This method has the advantage of revealing connectivity patterns on individual domains disentangled from a whole brain analysis. The dFDC is then analyzed using an information theory framework to assess the amount of information (in bits) shared among domains.

Dynamic Functional Domain Connectivity

Preprocessing and Estimation of Domains

Regular fMRI analysis requires a set of preprocessing steps. Depending on the type of analysis, these steps includes, but are not limited to, slice-timing correction, realignment, co-registration, spatial normalization, transformation to standard space, motion correction, and smoothing (Churchill and Strother, 2013; Power et al., 2014; Vergara et al., 2016). Preprocessed fMRI is then further analyzed to identify regions of interest in the brain and obtain their temporal behavior. Sets of distinctive brain networks have been identified (Allen

et al., 2011; Buckner et al., 2008; Raz, 2004; Shirer et al., 2012) and described by their spatial content and temporal behavior. We will denote the spatial content of these brain networks as S, which is a three dimensional image, and the temporal behavior as $X[t]$ where t designates discrete time. In the context of our approach, initial fMRI analysis delivers a set of networks $\mathbf{N}_M[t] = [(S_1, X_1[t]), (S_2, X_2[t]), \ldots (S_N, X_N[t])]$ describing spatio-temporal properties.

Identified brain networks are not isolated units. There is evidence that supports the concept of functionally interrelated brain networks (Rosazza and Minati, 2011; van den Heuvel et al., 2009). Based on the concept of brain areas having similar functional properties, we organize the set of all networks $\mathbf{N}_M[t]$ as a class containing subsets of functionally related networks such that $\mathbf{N}_M[t] = [\mathbf{N}^1[t], \mathbf{N}^2[t], \ldots, \mathbf{N}^M[t]]$. The subindex indicating subset size was dropped, but may be used if necessary. In several studies the subsets in $\mathbf{N}_M[t]$ are grouped according to anatomical and functional properties (Allen et al., 2011). The subsets $\mathbf{N}^i[t]$ in $\mathbf{N}_M[t]$ will be referred to as domains. In parallel with the function of specific brain regions, the definition and extent of the domains is a topic of evolving research. Examples of important functional domains found in the literature are sensorimotor, executive control, default mode, salience, visual, cerebellum and language (Shirer et al., 2012).

Dynamic Functional Domain Connectivity

The study of dynamic relationships between networks is achieved through the assessment of time-based connectivity using metrics such as coherence, correlation or covariance (Allen et al., 2012). Given a connectivity operator $o(\bullet,\bullet)$, the relationship R between two networks $(S_a, X_a[t])$ and $(S_b, X_b[t])$ will be denoted as $R_{a,b} = o(X_a[t], X_b[t])$. R has been estimated either by measuring over a sufficiently long period of time, which implies assumptions such as stationarity, or assessing the time evolution of coherence over shorter periods of time. Sliding windows (Chang and Glover, 2010) and wavelets (Yaesoubi et al., 2015) have been suggested through the literature to estimate the instantaneous coherence $R_{a,b}[t]$.

The dynamic study of brain domains starts with the assessment of the dynamic domain connectivity matrix $\boldsymbol{D}_{Z,Y}[t]$ containing all the instantaneous relationships $R_{Z,Y}[t]$ between the two domains $Z[t]$ and $Y[t]$. A clustering algorithm is applied to each $\boldsymbol{D}_{Z,Y}[t]$ separately, resulting in a set of κ clusters with centroids $\boldsymbol{C}^{\kappa}_{Z,Y} = [\boldsymbol{D}^1_{Z,Y}, \boldsymbol{D}^2_{Z,Y}, \ldots, \boldsymbol{D}^{\kappa}_{Z,Y}]$ and a membership function $m_{Z,Y}[t] \in \boldsymbol{C}^{\kappa}_{Z,Y}$. Each cluster contains information about a particular dynamic state in the dFDC. A similar procedure has been previously described (Allen et al., 2012) using the complete connectivity matrix. In contrast, this work applies clustering to connectivity submatrices defined by pairs of domains. Fig. 1 illustrates this procedural difference between dFNC and dFDC. The proposed procedure results in a total number of dFDCs determined by the possible number domain pairs.

Membership $m_{Z,Y}[t]$ indicates the closest cluster centroid at moment k estimated using an arbitrary distance measure $d(\bullet,\bullet)$. Examples of distance measures include L_1, L_2 norms and correlation. Similar to the procedure used in dFNC for the identification of whole brain dynamic states (Allen et al., 2012), the current dFDC method allows for the estimation of dynamic states at the domain level. States are characterized by the time-varying domain connectivity matrices $\boldsymbol{D}_{Z,Y}[t]$, algorithmically grouped into clusters with centroids $\boldsymbol{C}^{\kappa}_{Z,Y}$.

States and membership functions $m_{Z,Y}[t]$ are the base constituents of the dFDC analysis. Although initially defined for two different domains, the dFDC can also be assessed for a domain with itself resulting in a within domain dFDC.

Entropy and Mutual Information

It will be useful at this point to make an analogy with the concepts of information theory. Consider each of the dFDC states in the set $\boldsymbol{C}^{\kappa}{}_{Z,Y}$ as elements from an alphabet. State centroids in the set $\boldsymbol{C}^{\kappa}{}_{Z,Y}$ can aid in building a conceptual representation of this alphabet. The corresponding membership function $m_{Z,Y}[t]$ defines when and how frequently each dynamic state (alphabet element) appears. The membership function also allows us to make an estimate of the probability of a given state with centroid $\boldsymbol{D}^{i}{}_{Z,Y}$, which we will denote as $p^{i}_{Z,Y}$. This probability also indicates the occupancy rate of a particular state. Using $p^{i}_{Z,Y}$ we can calculate a dFDC entropy as

$$\mathrm{H}_{Z,Y} = -\sum\nolimits_{i} p^{i}_{Z,Y} \log p^{i}_{Z,Y} [\mathrm{bits/time\text{-}\ point}]. \quad (1)$$

In theory, entropy indicates the smallest number of bits necessary on average (using log base 2) to describe each time-point of the membership function. For example, assume that we are going to store the membership function in a digital memory device. According to concepts of data compression (Cover and Thomas, 2012), entropy indicates the smallest number of bits per time-point necessary to save the membership information in that memory device. Data compression algorithms rarely achieve enough efficiency to compress down to the entropy level. However, entropy is recognized as the amount of non redundant information contained in data. Entropy can also be used to measure uncertainty. At maximum entropy, all states are equally likely to be observed and thus indicate maximum uncertainty. This means that the membership for a random observation of the domain connectivity cannot be predicted. This also means that a large number of bits are necessary to describe all the possible outcomes of the membership function. In contrast, zero entropy indicates that one of the clusters is always the outcome, but the other ones have a zero probability of being observed. This case indicates a static membership that can be predicted because it does not change with time. Notice that all dynamic properties vanish in this extreme case of zero entropy degenerating to a static membership case with one single dFDC state. In our digital memory device example, there would be no need to store the outcome of the membership function.

Cross Domain Information Measure

We would like to estimate how much can be known about the connectivity between domains Z and Y given that connectivity between domains A and B is known. In many respects, this approach is similar to the relationship transmitter-receptor studied in communications which has been widely described using Information Theory (Tononi et al., 1998). The definition of the joint distribution is

$$p^{i,j}_{AB,ZY} = p(m_{Z,Y} = D^i_{Z,Y}\ ,\ \ m_{A,B} = D^j_{A,B})$$
$$D^i_{Z,Y} \in C^{\kappa_1}(Z,Y)\ ,\ \ D^j_{A,B} \in C^{\kappa_2}(A,B). \quad (2)$$

The estimation of $p^{i,j}_{AB,ZY}$ is based on the temporal co-occurrence of membership states in $m_{Z,Y}[t]$ and $m_{A,B}[t]$. In practice the joint probability can be calculated from frequency estimates. Adhering to the classical definition of mutual information, we define the cross domain mutual information (CDMI) measure $I_{AB,ZY}$ as

$$I_{AB,ZY} = \sum_{i,j} p^{i,j}_{AB,ZY} \log \frac{p^{i,j}_{AB,ZY}}{p^i_{A,B} p^j_{Z,Y}}. \quad (3)$$

Another measure that is readily available is the amount of independent information defined by the conditional entropy. For example $\mathrm{H}_{Z,Y|A,B}$ will be the amount of information between the domains Z and Y that does not depend on the connectivity between domains A and B. This calculation can be carried out by the simple equation:

$$\mathrm{H}_{Z,Y\big|A,B} = H_{Z,Y} - I_{AB,ZY}. \quad (4)$$

Methods

Subjects

Data from a total of 121 healthy subjects, 71 of which were female, was used for this study. The age of this cohort ranged from 18 to 53 years with mean and standard deviation of 25.4 ± 8.3. There was no significant difference in age between males and females after a two-sample t-test ($p>0.37$). Subjects did not exhibit injury to the brain, brain-related medical problems, bipolar or psychotic disorders, ADHD or a history of substance abuse/dependence including alcohol. All participants provided informed consent in accordance with institutional guidelines at the University of New Mexico.

Imaging

All images were collected on a 3 Tesla Siemens Trio scanner. A five-minute resting state run was completed by each participant using a single-shot, gradient-echo echo planar imaging sequence [TR = 2000 ms; TE = 29 ms; flip angle = 75°; FOV = 240 mm; matrix size = 64 × 64]. Foam padding and paper tape was used to restrict motion within the scanner. Thirty-three contiguous, axial 4.55 mm thick slices were selected to provide whole-brain coverage (voxel size: 3.75 × 3.75 × 4.55 mm). The first five images were eliminated to account for T1 equilibrium effects leaving a total of 145 images. Data were preprocessed using the statistical parametric mapping (http://www.fil.ion.ucl.ac.uk/spm) software (Friston, 2003). The preprocessing steps included slice-timing correction, realignment, co-registration,

spatial normalization and transformation to the Montreal Neurological Institute (MNI) standard space.

Time courses were orthogonalized with respect to i) linear, quadratic and cubic trends; ii) the six realignment parameters; iii) realignment parameters derivatives; and iv) spike regressors. The DVARS method (Power et al., 2012) was used to find spike regressors where the RMS exceeded three standard deviations. The fMRI data were smoothed using a FWHM Gaussian kernel of size 6 mm.

gICA and dFNC Preprocessing

The data were then analyzed with Infomax-based group independent component analysis (gICA) (Calhoun and Adali, 2012) with 120 and 100 components for the first and second decomposition levels respectively. A total of 42 components out of 100 estimated components were selected based on frequency content and visual inspection in order to include components that were low noise and free of major artifacts (Allen et al., 2011). The gICA time courses were then filtered using a band-pass filter from 0.01 to 0.15 Hz.

The set of RSNs were identified and grouped in their functional domains. Spatial overlap with functional brain areas were confirmed by visual comparison with the 90 spatial maps defined by Shirer (Shirer et al., 2012) and by running peak activation coordinates through the meta-analysis software publicly available at http://www.neurosynth.org/. The functional domains are SBC (Subcortical), CEB (Cerebellar), AUD (Auditory), SEN (Sensorimotor), VIS (Visual), SAL (Salience), DMN (Default Mode Network), ECN (Executive Control Network), LAN (Language) and PRC (Precuneus). Chosen RSNs have peak activations in grey matter, low spatial overlap with known vascular, ventricular, motion, and susceptibility artifacts.

dFDC

A total of 55 = (10*11)/2 dFDCs (unique pairs of functional domains) were obtained from the 10 domains under consideration. Of these, 10 dFDCs represent within domain (for example $\boldsymbol{D}_{DMN,DMN}[t]$). The other 45 dFDCs capture cross domain connectivity (for example $\boldsymbol{D}_{ECN,DMN}[t]$). On each of the 55 dFDCs, we used k-means clustering (Lloyd, 1982) with a correlation distance metric and a window size of 80 seconds. The number of clusters for each dFDC was set to three after using the elbow criterion on the cluster validity index (Allen et al., 2012).

State probabilities were estimated for all domains in each subject. Subject-wise probabilities are estimated using the state frequency designated by the membership function within each subject. Each of the state probabilities on each dFDC was subject to a linear model including age and sex. From a straightforward clustering point of view, these probabilities are simply cluster occupancy rates (adding to one over the three clusters in each dFDC). We regressed the dFDC probabilities on age and gender to understand how these probabilities are affected by demographic factors. The estimation of entropy summarizes the information from all states within the dFDC into only one value per subject and dFDC. From Eq. (1) it is clear that the maximum possible entropy value will be $\log_2$ (number of states in the dFDC). We

estimated CDMIs for all combinations of dFDCs and organized the values in matrix form. We also estimated the static functional network connectivity (sFNC) matrix to compare its structure with the CDMI matrix. In addition, relationships with age and sex were determined using subject-wise CDMI and a linear regression model.

Results

Fig. 2 displays mean state probabilities, averaged over the subject dimension, along with corresponding entropies calculated from the three mean state probabilities on each dFDC. Some dFDCs did not show preference for a given state. Specifically, the entropies of dFDCs SEN-SEN and VIS-VIS were very close to the maximum entropy achievable (1.585 bits) for three states. There were however many of the dFDC that exhibited a noticeable preference for one of the three states over the other two as indicated by the red color (high probability) in Fig. 2. The occurrence of preferred states lowers the value of entropy. However, the highest state preference (maximum probability of 0.56) was not strong enough to produce a large dynamic range of entropy.

Relationships with age and sex were tested for subject-wise entropy and state probabilities. Fig. 2 displays the results where increments and decrements of state probabilities are indicated by triangles in the case of age and arrows in the case of sex. More information about these linear regression results is provided in Supplementary Table I. Only the dFDC SBC-DMN showed a significant relationship with age. This increment is reflected in the significant change of state probabilities, making the three probabilities more similar. While the highest state probability decreases, the lowest state probability increases. There was no significant relationship of occupancy or entropy with sex on any dFDC.

We estimated the CDMI values using estimated single and joint probabilities from every pair of dFDCs as required by Eq. (3). Similar to what is done in previous functional connectivity analysis, we have organized the CDMI values in matrix form. The results for within dFDC mutual information, those within the same domain (for example SBC-SBC versus SBC-SBC) are not considered in this section. The reason is that within dFDC mutual information is equal to the entropy, $I(X; X) = H(X)$ (Cover and Thomas, 2012). The CDMI matrix is displayed in Fig. 3 where the main diagonal, composed of $I(X; X)$ type values, is set to zero. Excluding the main diagonal, there are 1485 off-diagonal mutual information computations ranging between 0 and 0.15 bits. Fig. 3 also displays the sFNC matrix for comparison.

In order to find which mutual information values, I, warrant further analysis, we bootstrapped the CDMI using 10^8 iterations and estimated significance thresholds. The threshold for a $p<0.01$ was estimated to be $I>0.094$ and for $p<0.05$ was $I>0.063$. After this, fifteen mutual information values passed the level $p<0.01$ as displayed in Fig. 4. Most of the surviving results were related to SBC and sensorimotor areas. In order to visualize the effect of having a relatively high I, we tested the ordered joint probabilities from significant ($p<0.01$) mutual information against the rest ($p>0.01$). As seen in Fig. 5, there is a significant difference between the two groups for the highest and lowest joint probabilities. This indicates that as mutual information grows there will be certain pairings of states with higher co-occurrence, which in turn increases the mutual information. For example, we have

identified the mutual information between SBC-DMN and SEN-VIS, which is significantly affected by age ($p<0.01$). The complete list of mutual information results related to age and sex is provided in Table I. We choose SBC-DMN vs. SEN-VIS because is the only pair of dFDCs in Table I that have all four different domains and thus can illustrate how two unrelated dFDCs influence each other. Fig. 6 displays the joint probabilities, spatial maps and state centroids. Two pairs of cross-domain states exhibit high joint probability with more than double the joint probabilities of the other seven co-occurring states.

Discussion

The current method establishes a framework to study information content in dynamic functional domain connectivity. Previous dynamic connectivity work (Allen et al., 2012), upon which we based our present study, considered whole brain clustering. Instead, the current approach addresses dynamic connectivity at the functional domain level including domain connectivity patterns and mutual information measures. Our current proposal does not intend to specify the baseline functional connectivity method employed. For example, instead of gICA (Calhoun and Adali, 2012), atlas based methods (Shirer et al., 2012) may be used as well in finding timecourses. For our current work, we selected gICA to have a more data-driven approach. Although we have utilized clustering, other alternatives such as PCA (Leonardi et al., 2013) exist; however, a full comparison among different approaches is outside of the scope of this paper. This last remark, also applies to the parameter set of the current analysis. The parameter set was chosen for stability based on previous work suggesting to filter frequencies higher than 0.15 Hz, apply a window size in the range of 30 to 120 seconds, and use 100 components for gICA (Allen et al., 2012). Further advances in dFNC provide highly refined whole brain techniques including time-frequency coherence (Yaesoubi et al., 2015) and weighted dynamic connectivity (Miller et al., 2016b). Future work may incorporate these and other important techniques into the study of domain connectivity, providing a more detailed characterization of dynamic connectivity than is possible with whole brain analyses.

One of the basic goals of applying information theory to dFDCs is to determine the amount of information carried in the dynamic succession of states at the domain level. Our results indicate that the amount of information is typically close to the maximum that can be theoretically expected (i.e., the maximum entropy). These high entropies point toward a highly dynamic system with much information content. Results also suggest a highly unpredictable system in which the underlying language for single dFDCs (assuming decoding is possible) is very difficult to infer. Nevertheless, the dependency of entropy on age found between the SBC and DMN domains suggests an increase on the number of bits required to describe the dFDC through the aging process. The two SBC and DMN domains involve brain regions (see Fig. 6) with important roles in fMRI resting state studies. The SBC brain areas are known to be affected in patients of attention deficit hyperactivity disorder (Cao et al., 2009), major depression (Greicius et al., 2007; He et al., 2016), schizophrenia (Rashid et al., 2016) and other disorders during resting state. The DMN domain is fundamental for resting state brain function (Buckner et al., 2008). The significant increase of entropy indicates a disruption where preferred dynamic states are less probable to occur. At a basic level, entropy is a nonlinear summary measure that can be used as an

alternative to linear summaries such as averaging. However, the semantic behind entropy is directly related to amounts of information. Particularly, the mechanism behind increments of entropy and lack of state preference is related to changes of information shared with other dFDCs. This is exemplified by the increase of CDMI in relation to age (details available in Table I) observed between SBC-DMN (the dFDC significantly related to age) and other dFDCs including SEN-VIS, SAL-SAL and ECN-LAN. First, the resting state activity of the DMN is known to reduce with normal aging (Damoiseaux et al., 2008). Second and in addition to the DMN, the disruption produced during normal aging involves other brain areas including the salience network (in our data represented by the SAL domain) and the fronto-parietal network (Marstaller et al., 2015), which is an integral part of the ECN. In our data, the increments of CDMI with age suggest a recruitment of information into the SBC-DMN from other important dFDCs such as SAL and ECN that in contrast to the DMN are not involved in self-referential activity. A possible explanation includes the need of more information from other brain areas as a mechanism of compensation due to reduced DMN activity. In relation to sex, the dFDC CER-CER also shows different CDMI in SEN-SEN, SEN-VIS and DMN-LAN. Differences between cerebellum and motor areas are known to exist between the sexes (Ingalhalikar et al., 2014). However, this did not produce a difference in entropy for the CER-CER dFDC. The mechanism producing this CDMI difference in CER-CER might vary from the one acting in SBC-DMN. Although our study does not focus on such questions, obtained results indicate that the proposed information theoretic framework is sensitive to changes in uncertainty and information flow among domains.

Moving beyond the results for single dFDC entropy, the CDMI results show a more predictable pattern of information sharing (measured in bits) among the dFDCs. Observed CDMI patterns exhibit similarities with the arrangement of sFNC matrices and provides validation for the observed configuration of the CDMI matrix. These similarities emerge when comparing subcortical, sensorimotor and cerebellum areas. SBC related dFDCs have strong CDMI values with other dFDC containing SBC (SBC-CER, SBC-AUD, etc.), which can be compared to existing static connectivity between SBC and the other domains (see Fig. 3 and Fig. 4). Also similar to static connectivity is the noticeable cluster of sensorimotor, visual and cerebellum areas. In spite of both matrices displaying different types of measures, the comparison indicates some overlap between strong functional connectivity and relatively high number of bits shared across domains. However, the differences also indicate that neither measure implies the other. Although not completely absent, there is a noticeable lack of strong mutual information among SAL, ECN, DMN, LAN and PRC domains. These observations suggest that, in spite of notable similarities, functional connectivity does not provide the same type of information as CDMI. CDMI has its own characteristics that enhance our ability to analyze the brain.

CDMI results may be related to known information pathways in the brain. The main components of the SBC domain are the putamen and the thalamus, two important brain areas of information relay belonging to the cortico-striatal loops (Alexander et al., 1986). One fundamental question is whether information is processed in parallel or if there is some sort of funneling in where data arriving from different cortical areas then intermix (Parent and Hazrati, 1995). In the case of parallel processing, dFDCs excluding the SBC domain (for

example SEN-SEN, SEN-VIS, CER-ECN and other similar dFDCs) would be able to share information with the SBC-SBC dFDC influencing membership probabilities. If this were the case, then unrelated dFDCs would compete for access to the SBC domain and affect its connectivity. However, Fig. 4 shows no evidence of this outcome. CDMI is strong and frequent among dFDCs that include the SBC domain (e.g., SBC-LAN, SBC-ECN, SBC-DMN, etc.) forming the SBC cluster in the superior-left corner of Fig. 3 and Fig. 4. This SBC cluster supports the hypothesis of interaction among the different connections between cortical areas and the striatum (Parent and Hazrati, 1995). In this scenario, it is more feasible that a domain X affects the membership of the SBC-SBC dFDC only though its connection dFDC X-SBC dFDC. Furthermore, information overlap is exemplified by the CDMI between dFDCs with SBC as a common node such as the strong CDMI between SBC-SEN and SBC-PRC displayed in Fig. 4. The SBC case is not unique in Fig. 4; the dFDCs in the sensorimotor cluster (dFDCs involving the AUD, SEN, VIS, and CER domains) follow a similar CDMI pattern, suggesting that information overlap might be a common mechanism.

At the other end of the spectrum, the CDMIs for networks other than SBC and sensorimotor were rarely significant. This reduced communication could be linked to the resting state nature of the data. Specifically, it is plausible that ECN (Seeley et al., 2007) and DMN (Raichle, 2015) domains do not require a significant amount of CDMI bits since the ECN might not be particularly required during the resting state, while the DMN is known to be active in the absence of explicit tasks (Fox et al., 2005). This argument does not imply a direct relationship between activity and CDMI, but as with the case of phase in sFNC measures, activity might have some effect on CDMI. Reduced and absent CDMI among dFDCs might result from lack of activity exhibited by data acquired during subjects resting state.

The two CDMI patterns discussed suggest the existence of two different processes happening during resting state. One process is exogenous in nature involving communication among areas dedicated to input signals. The other process is endogenous with little communication among domains, as evidenced by the scarcity of significant CDMIs, but with high information content since information values were always high within domains (i.e., dFDCs exhibit high entropy). This bipartite observation is in line with the hypothesis of two default modes in brain function proposed previously (Fransson, 2005). One mode drives the self-referential mental activity anchored at the DMN (Greicius et al., 2003; Raichle, 2015). The other mode interrupts self-referential activity and temporary shifts into an extrospective state of mind. This extrospection maintains readiness in case attention to the outside environment is necessary (Fransson, 2005). Other studies have also provided evidence of dual resting state modes where activation can be influenced even when subjective attention and control is voluntarily enforced (Van Calster et al., 2016). Most conclusions found in the literature are based on anti-correlations between brain networks, but the functional significance of these results is not fully understood yet (Chen et al., 2017). The contribution of this CDMI study indicates that there is limited data exchange between brain domains of endogenous self-referential and exogenous attention control and readiness. Albeit high data processing activity may occurs continuously within each functional domain.

One broad finding that comes from computing CDMI is that the number of bits shared across the brain is rather small. For example, the CDMI of Fig. 6 (SBC-DMN vs. SEN-VIS) only have about 0.061 bits, but this low amount of information is no surprise. Considering that each of the 55 dFDCs can share its approximately 1.585 bits (maximum entropy) with the other 54 dFDCs, an even distribution of CDMI results in an assignment of 0.03 bits for each dFDC. The CDMI of Fig. 6 doubles this quantity, which by comparison does not seem small. Furthermore, the maximum CDMI observed is five times the hypothetical 0.03 bits. Fig. 5 and Fig. 6 clearly illustrate the effect that small CDMI values can have over the dynamic states. A CDMI of 0.15 will increase the value of some joint probabilities and decrease some others such that observing a state in one dFDC increases the probability of determining the state of another dFDC. This is the case of Fig. 6 where the chances are as high as 24% of the time. Based on this discussion, it is normal to expect small CDMI values.

An assumption in our framework that has advantages and disadvantages is that brain networks have been correctly organized in functional domains. There is considerable evidence for the existence of this domain organization. One of the most studied domains is the DMN (Buckner et al., 2008), which has been the main focus in studying many diseases (Garrity et al., 2007; Zhou et al., 2012). It is critical for our method that domains are correctly organized around functionally related networks. However, the order can be different depending on the context of each study. Grouping appropriateness is an evolving topic in the literature (Buckner et al., 2008; Fox et al., 2005; Shirer et al., 2012; van den Heuvel et al., 2009). In applying the method presented, it is important to keep in mind that results are dependent upon the predefined domains. The current approach suffers from several of the issues that have also limited dFNC analysis. Some of these issues are related to physiological noise, preprocessing, clustering and window length. In our case, we assume that data processing, including all steps taken for windowing and clustering, were correct and stable. We also have to consider that different clustering methods, connectivity and distance metrics can change the final results. One detail left for future work is the search for the underlying code driving the communication of bits among dFDCs. Our presented results provide evidence for the existence of such a code based on shared information bits. For example, the two pairs of states (1,1) and (1,2) which occur more frequently in Fig. 6 might be the key components of a code used between the dFDCs SBC-DMN and SEN-VIS. The estimation of such a communication code will require further investigation and development of new techniques.

Supplementary Material

Refer to Web version on PubMed Central for supplementary material.

Acknowledgments

This work was supported by the National Institutes of Health [grant numbers P20GM103472, 1R01EB006841, R01EB020407]; and the National Science Foundation [grant number #1539067] to V.C.

References

Alexander GE, DeLong MR, Strick PL. Parallel organization of functionally segregated circuits linking basal ganglia and cortex. Annual review of neuroscience. 1986; 9:357–381.

Allen EA, Damaraju E, Plis SM, Erhardt EB, Eichele T, Calhoun VD. Tracking whole-brain connectivity dynamics in the resting state. Cerebral cortex. 2012:bhs352.

Allen EA, Erhardt EB, Damaraju E, Gruner W, Segall JM, Silva RF, Havlicek M, Rachakonda S, Fries J, Kalyanam R, Michael AM, Caprihan A, Turner JA, Eichele T, Adelsheim S, Bryan AD, Bustillo J, Clark VP, Feldstein Ewing SW, Filbey F, Ford CC, Hutchison K, Jung RE, Kiehl KA, Kodituwakku P, Komesu YM, Mayer AR, Pearlson GD, Phillips JP, Sadek JR, Stevens M, Teuscher U, Thoma RJ, Calhoun VD. A baseline for the multivariate comparison of resting-state networks. Front Syst Neurosci. 2011; 5:2. [PubMed: 21442040]

Buckner RL, Andrews-Hanna JR, Schacter DL. The brain's default network. Annals of the New York Academy of Sciences. 2008; 1124:1–38. [PubMed: 18400922]

Calhoun VD, Adali T. Multisubject independent component analysis of fMRI: a decade of intrinsic networks, default mode, and neurodiagnostic discovery. Biomedical Engineering, IEEE Reviews in. 2012; 5:60–73.

Cao X, Cao Q, Long X, Sun L, Sui M, Zhu C, Zuo X, Zang Y, Wang Y. Abnormal resting-state functional connectivity patterns of the putamen in medication-naive children with attention deficit hyperactivity disorder. Brain research. 2009; 1303:195–206. [PubMed: 19699190]

Chang C, Glover GH. Time–frequency dynamics of resting-state brain connectivity measured with fMRI. Neuroimage. 2010; 50:81–98. [PubMed: 20006716]

Chen JE, Glover GH, Greicius MD, Chang C. Dissociated patterns of anti-correlations with dorsal and ventral default-mode networks at rest. Human brain mapping. 2017

Churchill NW, Strother SC. PHYCAA+: an optimized, adaptive procedure for measuring and controlling physiological noise in BOLD fMRI. Neuroimage. 2013; 82:306–325. [PubMed: 23727534]

Cover, TM., Thomas, JA. Elements of information theory. John Wiley & Sons; 2012.

Damoiseaux J, Beckmann C, Arigita ES, Barkhof F, Scheltens P, Stam C, Smith S, Rombouts S. Reduced resting-state brain activity in the "default network" in normal aging. Cerebral cortex. 2008; 18:1856–1864. [PubMed: 18063564]

Erhardt EB, Rachakonda S, Bedrick EJ, Allen EA, Adali T, Calhoun VD. Comparison of multi-subject ICA methods for analysis of fMRI data. Human brain mapping. 2011; 32:2075–2095. [PubMed: 21162045]

Fox MD, Greicius M, Fox M, Greicius M. Clinical applications of resting state functional connectivity. Frontiers in systems neuroscience. 2010; 4:19. [PubMed: 20592951]

Fox MD, Snyder AZ, Vincent JL, Corbetta M, Van Essen DC, Raichle ME. The human brain is intrinsically organized into dynamic, anticorrelated functional networks. Proceedings of the National Academy of Sciences of the United States of America. 2005; 102:9673–9678. [PubMed: 15976020]

Fransson P. Spontaneous low-frequency BOLD signal fluctuations: An fMRI investigation of the resting-state default mode of brain function hypothesis. Human brain mapping. 2005; 26:15–29. [PubMed: 15852468]

Friston, KJ. Neuroscience Databases. Springer; 2003. Statistical parametric mapping; p. 237-250.

Garrity AG, Pearlson GD, McKiernan K, Lloyd D, Kiehl KA, Calhoun VD. Aberrant "default mode" functional connectivity in schizophrenia. 2007

Greicius MD, Flores BH, Menon V, Glover GH, Solvason HB, Kenna H, Reiss AL, Schatzberg AF. Resting-state functional connectivity in major depression: abnormally increased contributions from subgenual cingulate cortex and thalamus. Biological psychiatry. 2007; 62:429–437. [PubMed: 17210143]

Greicius MD, Krasnow B, Reiss AL, Menon V. Functional connectivity in the resting brain: a network analysis of the default mode hypothesis. Proceedings of the National Academy of Sciences. 2003; 100:253–258.

He H, Yu Q, Du Y, Vergara V, Victor TA, Drevets WC, Savitz JB, Jiang T, Sui J, Calhoun VD. Resting-state functional network connectivity in prefrontal regions differs between unmedicated patients with bipolar and major depressive disorders. J Affect Disord. 2016; 190:483–493. [PubMed: 26551408]

Ingalhalikar M, Smith A, Parker D, Satterthwaite TD, Elliott MA, Ruparel K, Hakonarson H, Gur RE, Gur RC, Verma R. Sex differences in the structural connectome of the human brain. Proceedings of the National Academy of Sciences. 2014; 111:823–828.

Leonardi N, Richiardi J, Gschwind M, Simioni S, Annoni JM, Schluep M, Vuilleumier P, Van De Ville D. Principal components of functional connectivity: a new approach to study dynamic brain connectivity during rest. Neuroimage. 2013; 83:937–950. [PubMed: 23872496]

Lloyd S. Least squares quantization in PCM. IEEE transactions on information theory. 1982; 28:129–137.

Marstaller L, Williams M, Rich A, Savage G, Burianová H. Aging and large-scale functional networks: White matter integrity, gray matter volume, and functional connectivity in the resting state. Neuroscience. 2015; 290:369–378. [PubMed: 25644420]

Miller RL, Vergara V, Keator DB, Calhoun VD. A Method for Inter-temporal Functional Domain Connectivity Analysis: Application to Schizophrenia Reveals Distorted Directional Information Flow. IEEE Transactions on Biomedical Engineering. 2016a in press.

Miller RL, Yaesoubi M, Turner JA, Mathalon D, Preda A, Pearlson G, Adali T, Calhoun VD. Higher Dimensional Meta-State Analysis Reveals Reduced Resting fMRI Connectivity Dynamism in Schizophrenia Patients. PloS one. 2016b; 11:e0149849. [PubMed: 26981625]

Parent A, Hazrati LN. Functional anatomy of the basal ganglia. I. The cortico-basal ganglia-thalamo-cortical loop. Brain Research Reviews. 1995; 20:91–127. [PubMed: 7711769]

Power JD, Barnes KA, Snyder AZ, Schlaggar BL, Petersen SE. Spurious but systematic correlations in functional connectivity MRI networks arise from subject motion. Neuroimage. 2012; 59:2142–2154. [PubMed: 22019881]

Power JD, Mitra A, Laumann TO, Snyder AZ, Schlaggar BL, Petersen SE. Methods to detect, characterize, and remove motion artifact in resting state fMRI. Neuroimage. 2014; 84:320–341. [PubMed: 23994314]

Raichle ME. The brain's default mode network. Annual review of neuroscience. 2015; 38:433–447.

Rashid B, Arbabshirani MR, Damaraju E, Cetin MS, Miller R, Pearlson GD, Calhoun VD. Classification of schizophrenia and bipolar patients using static and dynamic resting-state fMRI brain connectivity. Neuroimage. 2016; 134:645–657. [PubMed: 27118088]

Raz A. Anatomy of attentional networks. The Anatomical Record Part B: The New Anatomist. 2004; 281:21–36.

Rosazza C, Minati L. Resting-state brain networks: literature review and clinical applications. Neurological Sciences. 2011; 32:773–785. [PubMed: 21667095]

Sakoğlu Ü, Pearlson GD, Kiehl KA, Wang YM, Michael AM, Calhoun VD. A method for evaluating dynamic functional network connectivity and task-modulation: application to schizophrenia. Magnetic Resonance Materials in Physics, Biology and Medicine. 2010; 23:351–366.

Seeley WW, Menon V, Schatzberg AF, Keller J, Glover GH, Kenna H, Reiss AL, Greicius MD. Dissociable intrinsic connectivity networks for salience processing and executive control. Journal of Neuroscience. 2007; 27:2349–2356. [PubMed: 17329432]

Shirer W, Ryali S, Rykhlevskaia E, Menon V, Greicius M. Decoding subject-driven cognitive states with whole-brain connectivity patterns. Cerebral cortex. 2012; 22:158–165. [PubMed: 21616982]

Sutherland MT, McHugh MJ, Pariyadath V, Stein EA. Resting state functional connectivity in addiction: lessons learned and a road ahead. Neuroimage. 2012; 62:2281–2295. [PubMed: 22326834]

Tononi G, Edelman GM, Sporns O. Complexity and coherency: integrating information in the brain. Trends in cognitive sciences. 1998; 2:474–484. [PubMed: 21227298]

Van Calster L, D'Argembeau A, Salmon E, Peters F, Majerus S. Fluctuations of attentional networks and default mode network during the resting state reflect variations in cognitive states: Evidence from a novel resting-state experience sampling method. Journal of Cognitive Neuroscience. 2016

van den Heuvel MP, Mandl RC, Kahn RS, Pol H, Hilleke E. Functionally linked resting-state networks reflect the underlying structural connectivity architecture of the human brain. Human brain mapping. 2009; 30:3127–3141. [PubMed: 19235882]

Vergara VM, Mayer AR, Damaraju E, Hutchison K, Calhoun VD. The effect of preprocessing pipelines in subject classification and detection of abnormal resting state functional network connectivity using group ICA. Neuroimage. 2016

Yaesoubi M, Allen EA, Miller RL, Calhoun VD. Dynamic coherence analysis of resting fMRI data to jointly capture state-based phase, frequency, and time-domain information. Neuroimage. 2015; 120:133–142. [PubMed: 26162552]

Zhou Y, Milham MP, Lui YW, Miles L, Reaume J, Sodickson DK, Grossman RI, Ge Y. Default-mode network disruption in mild traumatic brain injury. Radiology. 2012; 265:882–892. [PubMed: 23175546]

Highlights

- An Information Theory Framework for Dynamic Functional Domain Connectivity
- Functional domains (groups of brain networks) share information with each other.
- As in communication theory, information can be measured in bits using entropy.
- The entropy metric utilizes the dynamic succession of connectivity states.
- Results provide evidence for mutual information links among brain areas.
- The manuscript defines an information theory framework for functional connectivity.

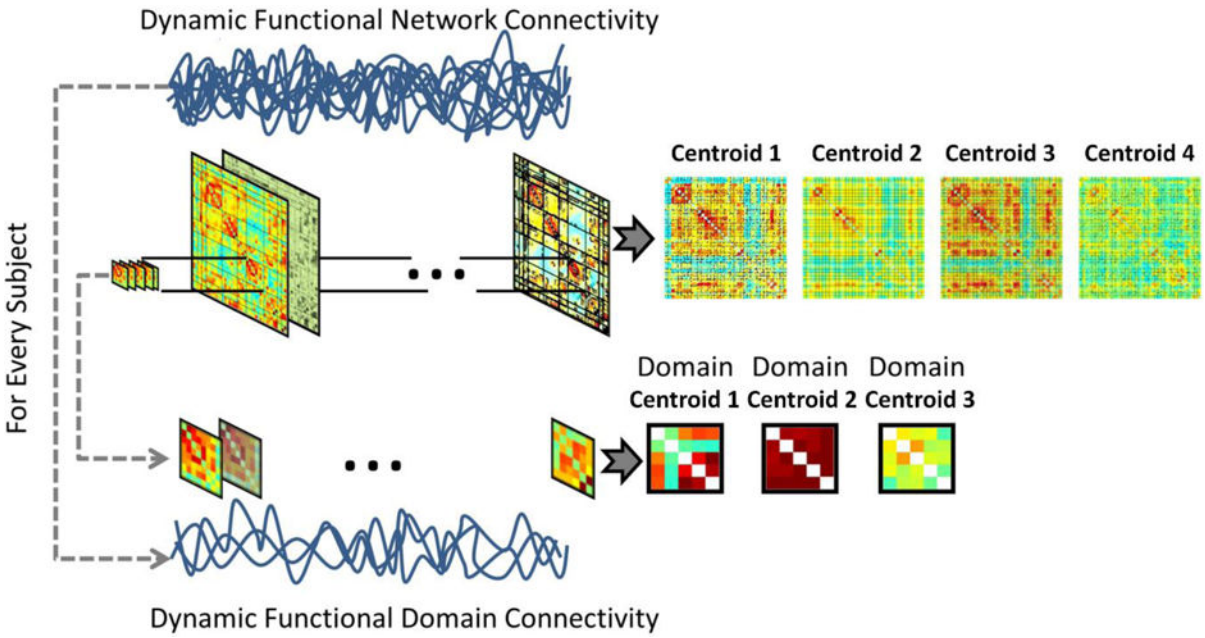

Fig. 1.

The same clustering technique used in dFNC is also used in dFDC to cluster data from domain pairs. The difference strives in the use of submatrices instead of the whole functional connectivity matrix.

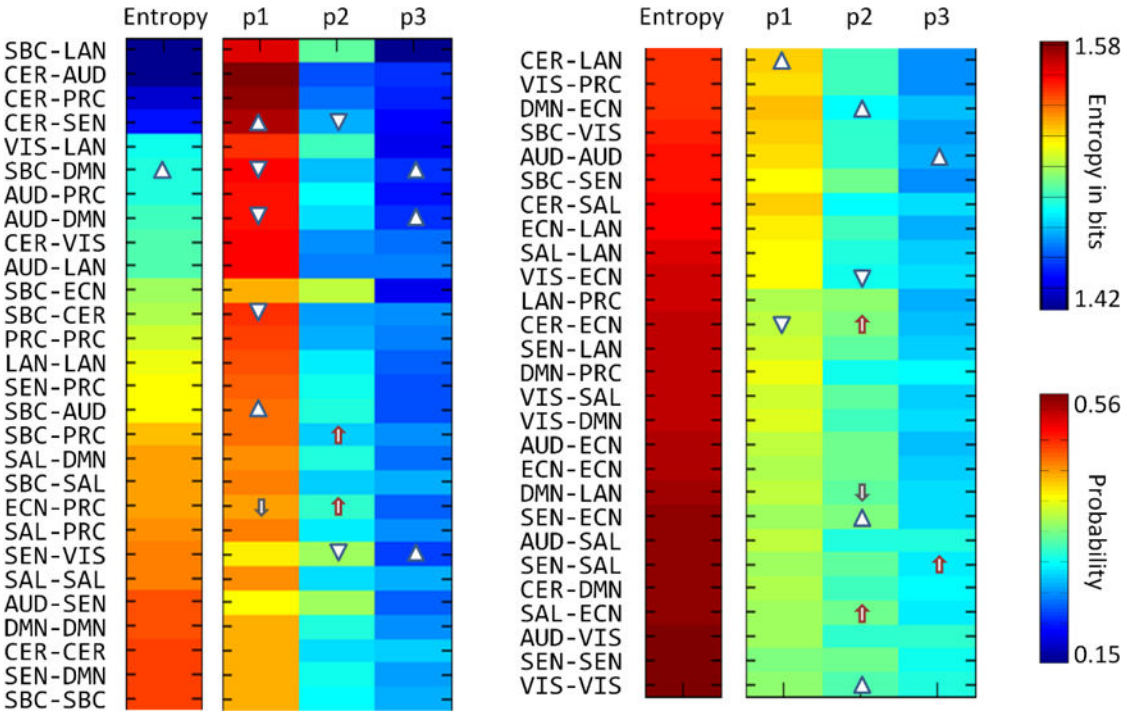

Fig. 2.

Entropy and cluster probability results. Triangles and arrows facing upward and downwards indicate significant increment and decrement related to age and sex correspondingly. There was no significant relationship with sex. Significance was assessed at $p<0.01$. Completely random situations are described by an entropy value of 1.58.

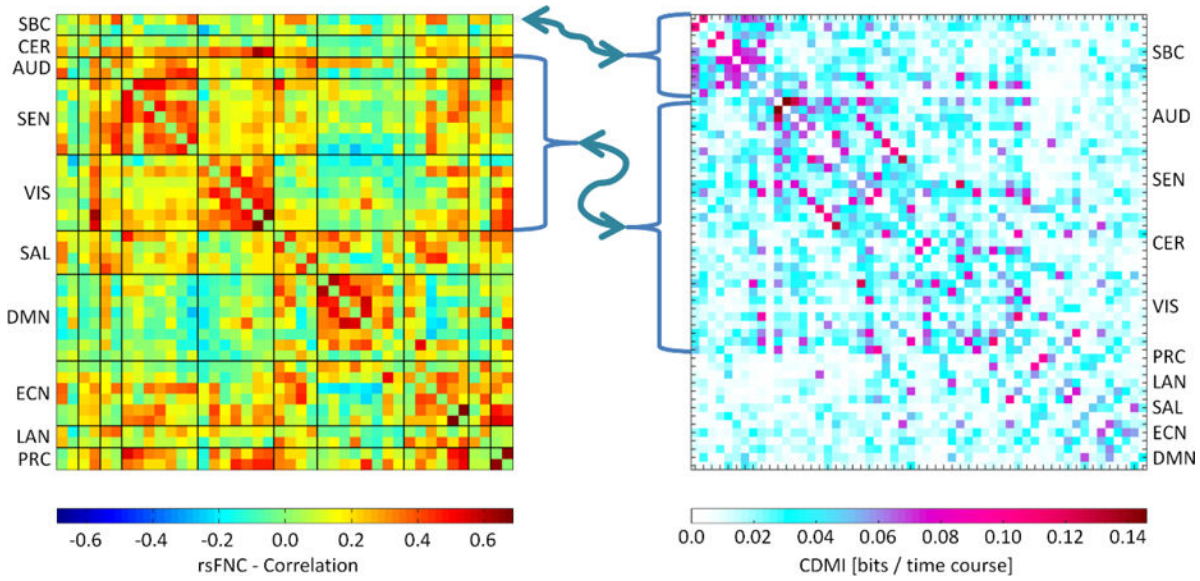

Fig. 3.

This figure compares sFNC and mutual information matrices. Both matrices show a similar relationship among SEN, VIS, AUD and CER domains. Also, the SBC domain exhibits a strong connection and mutual information with other domains in both matrices. The patterns are different in the case of DMN, ECN, LAN, SAL and PRC domains.

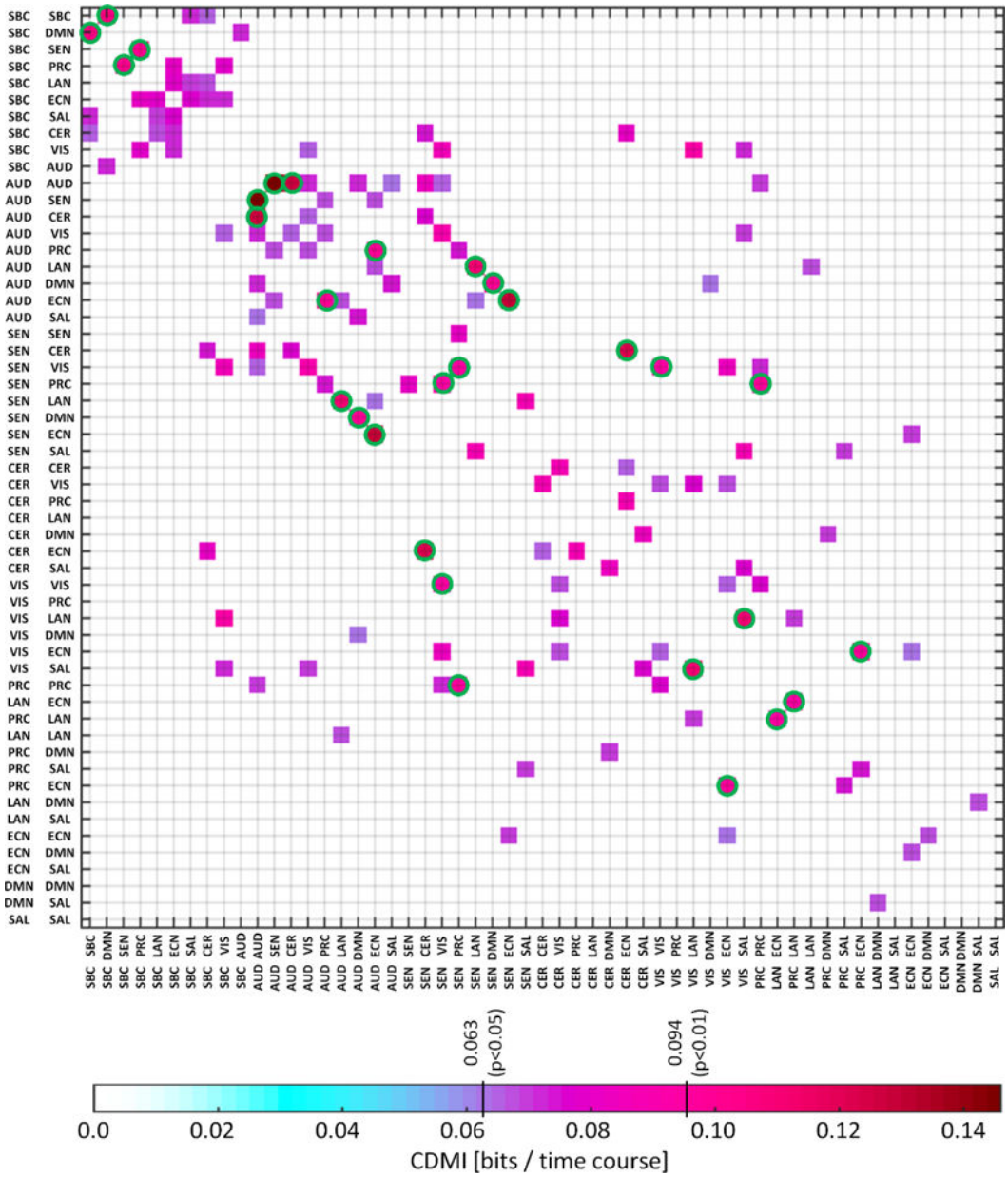

Fig. 4.

Mutual information matrix displaying values complying two different significant thresholds: $p<0.05$ and $p<0.01$. Mutual information was bootstrapped to obtain the p-value thresholds. Green circles display 15 points with $p<0.01$. The points where $p<0.05$ are displayed to better illustrate the matrix structure where the SBC domain have strong within mutual information. The other noticeable pattern is the appearance of strong mutual information within and among cerebellum, sensorial and motor domains.

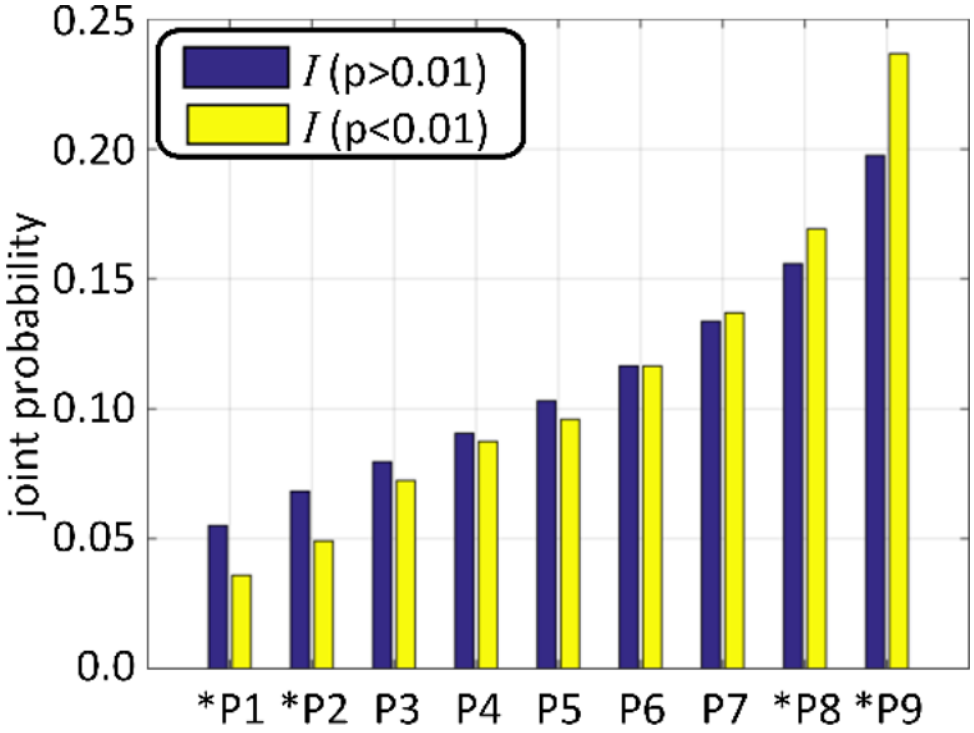

Fig. 5.

This figure illustrates the differences of joint probability values between those passing the $p<0.01$ threshold and those that do not pass. The nine joint probabilities (since there are three dynamic states per dFDC) of ally dFDC pairs were sorted in ascending order. The two largest probabilities were significantly higher ($p<0.01$) for the group of 15 cross domain information measures with $p<0.01$ (displayed with green circles in Fig. 4) compared to the rest. In addition, the two smallest joint probabilities were significantly lower. This difference explains the enhanced cross domain information measure observed.

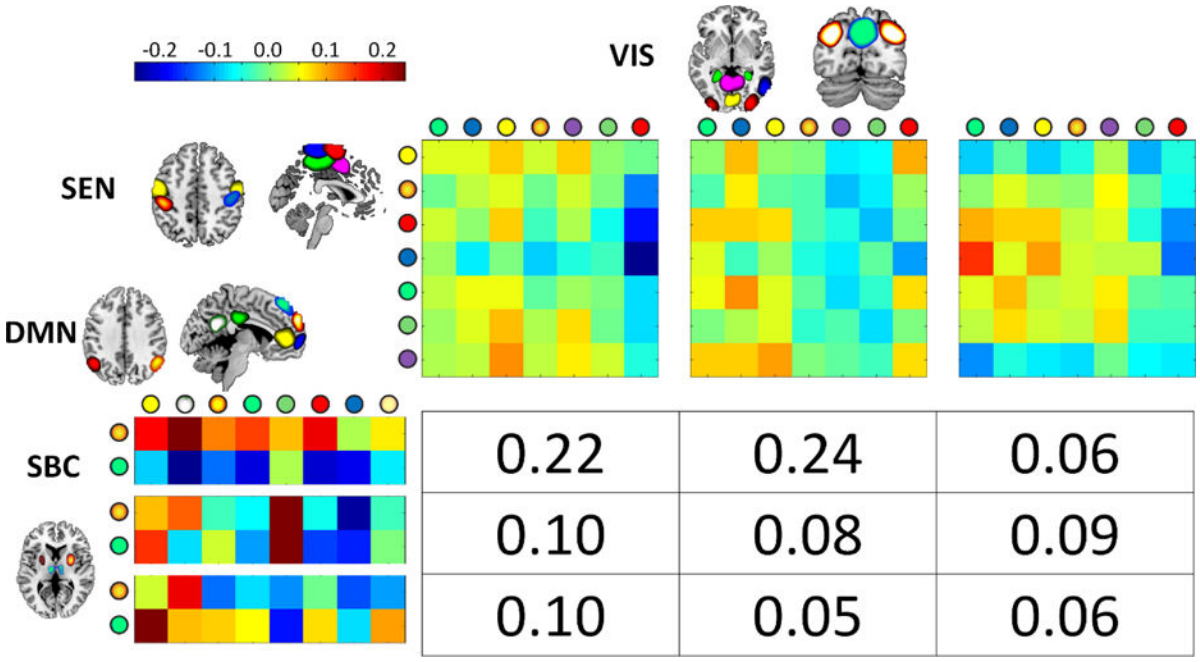

Fig. 6.

Displayed result was selected from the set that showed significant relationships with considered covariant. The cross domain information for SBC-DMN vs. SEN-VIS (mean I=0.06) showed significant increment with age (beta = 0.0063 and p=0.0018). The circles on the state centroids axis designate the brain region displayed. The two joint probabilities 0.22 and 0.24 drive the cross information measure since both are similarly larger than the rest.

Table I

List of CDMIs having significant relationship with sex (*) or age (**).

pair1	Pair2	I	H1	H2	sexbeta	sexpval	agebeta	agepval
SBC-CER	ECN-LAN	0.0050	1.5019	1.5591	0.0566	0.1072	0.0055	**0.0096
SBC-CER	LAN-PRC	0.0044	1.5019	1.5684	0.0208	0.5453	0.0069	**0.0010
SBC-DMN	SEN-VIS	0.0606	1.4752	1.5357	−0.0439	0.1832	0.0063	**0.0018
SBC-DMN	SAL-SAL	0.0018	1.4752	1.5369	−0.0008	0.9831	0.0081	**0.0003
SBC-DMN	ECN-LAN	0.0037	1.4752	1.5591	0.0219	0.5183	0.0053	**0.0094
SBC-LAN	CER-VIS	0.0057	1.4055	1.4845	−0.0201	0.5005	−0.0050	**0.0058
SBC-LAN	SAL-LAN	0.0311	1.4055	1.5653	−0.0964	*0.0058	−0.0026	0.2010
CER-CER	SEN-SEN	0.0222	1.5470	1.5821	−0.1020	*0.0037	−0.0012	0.5625
CER-CER	SEN-VIS	0.0068	1.5470	1.5357	−0.0864	*0.0044	0.0026	0.1391
CER-CER	DMN-LAN	0.0011	1.5470	1.5744	−0.0820	*0.0085	0.0020	0.2875
CER-VIS	VIS-ECN	0.0678	1.4845	1.5664	−0.0256	0.4568	−0.0054	**0.0100
CER-PRC	SAL-DMN	0.0042	1.4187	1.5307	−0.0917	*0.0051	−0.0026	0.1830
AUD-SEN	SAL-SAL	0.0073	1.5445	1.5369	−0.0139	0.6837	0.0055	**0.0075
AUD-SAL	SEN-VIS	0.0124	1.5782	1.5357	−0.1076	*0.0037	0.0044	0.0428
SEN-VIS	SAL-SAL	0.0151	1.5357	1.5369	−0.0550	0.1297	0.0061	**0.0051
SEN-VIS	SAL-ECN	0.0337	1.5357	1.5791	−0.0534	0.1162	0.0056	0.0064
SEN-PRC	VIS-ECN	0.0182	1.5140	1.5664	0.0003	0.9935	−0.0051	**0.0098
SAL-DMN	DMN-LAN	0.0678	1.5307	1.5744	−0.1215	*0.0025	−0.0020	0.4030
DMN-DMN	LAN-PRC	0.0080	1.5446	1.5684	0.0944	*0.0031	−0.0011	0.5615
DMN-ECN	ECN-ECN	0.0679	1.5519	1.5739	0.1076	*0.0069	0.0024	0.2995

J Neurosci Methods. Author manuscript; available in PMC 2018 June 01.